Carbohydrate Polymers 324 (2024) 121475

Contents lists available at ScienceDirect

Carbohydrate Polymers

journal homepage: www.elsevier.com/locate/carbpol

Covalent connectivity of glycogen in brewer's spent yeast cell walls revealed by enzymatic approaches and dynamic nuclear polarization NMR

Rita Bastos [a], Ildefonso Marín-Montesinos [b,*], Sónia S. Ferreira [a], Frédéric Mentink-Vigier [c], Mariana Sardo [b], Luís Mafra [b], Manuel A. Coimbra [a], Elisabete Coelho [a,*]

[a] LAQV-REQUIMTE, Department of Chemistry, University of Aveiro, 3810-193 Aveiro, Portugal
[b] CICECO-Aveiro Institute of Materials, Department of Chemistry University of Aveiro, 3810-193 Aveiro, Portugal
[c] National High Magnetic Field Laboratory, Florida State University, Tallahassee, 32310, FL, United States

ARTICLE INFO

Keywords:
Brewing
Glucan
Enzymatic hydrolysis
NMR
MAS-DNP
Ionic chromatography

ABSTRACT

Yeast cell walls undergo modifications during the brewing process, leading to a remodelling of their architecture. One significant change is the increased insolubility of the cell wall glycogen pool, likely due to the formation of covalent bonds between glycogen and cell wall polysaccharides. To verify this hypothesis, we extracted the brewer's spent yeast with 4 M KOH, obtaining an insoluble glucan fraction (AE.4 M) primarily composed of (α1 → 4)- and (1 → 3)-linked Glc residues. Dynamic nuclear polarization solid-state NMR of AE.4 M revealed distinct glucan resonances that helped to differentiate between α- and β glucosyl (1 → 4)-linked residues, and confirm covalent linkages between (β1 → 3)-glucans and glycogen through a (β1 → 4)-linkage.

The hydrolysis with different *endo*-glucanases (zymolyase, cellulase, and lichenase) was used to obtain solubilized high molecular weight glycogen fractions. NMR analysis showed that covalent links between glycogen and (β1 → 6)-glucans through (α1 → 6) glycosidic linkage, with branching at the C6 position involving (β1 → 3), and (β1 → 6)-glucans. HPAEC-PAD analysis of the enzymatically released oligosaccharides confirmed covalent linkages of (β1 → 3), (β1 → 6)-, and (β1 → 4)-glucan motifs with (α1 → 4)-glucans. This combination of multiple enzymatic approaches and NMR methods shed light into the role of yeast cell wall glycogen as a structural core covalently linked to other cell wall components during the brewing process.

1. Introduction

Brewer's yeasts, mainly from Saccharomyces genus, are unicellular fungi used in beer brewing. In modern brewing, yeasts are often subjected to repitching and reused across multiple generations, increasing their stress (Gibson et al., 2007). To mitigate the effect of stressful conditions, the cell wall is crucial to protect yeasts from the environmental changes (Aguilar-Uscanga & François, 2003; Klis et al., 2006). It acts as a physicochemical barrier capable to adapt to various stimuli, enhancing yeast resistance and survival during brewery handling (Bastos et al., 2015; Gibson et al., 2007).

The cell wall of Saccharomyces represents ~25 % of its dry weight, primarily composed of polysaccharides (up to 90 %). This architecture is organized in layers, including an outer fibrillar layer consisting of α-mannoproteins and an inner skeletal layer of chitin and glucans (Bastos et al., 2022). Glucans account for 30–60 % of the cell wall dry weight, composed of polysaccharides linked through (β1 → 3)- and (β1 → 6)-D-Glc linkages (β-glucans), as well as polysaccharides linked through (α1 → 4)-D-Glc linkages branched at (α1 → 4,6)-D-Glc (α-glucans), referred as cell wall glycogen (Bastos et al., 2015; Bastos et al., 2022; Kwiatkowski et al., 2009). While β-glucans are recognized for providing strength to maintain the cell wall integrity, the role of glycogen in cell wall architecture and function remains unclear. Previous works report its involvement in the cell osmotic tolerance (Lillie & Pringle, 1980), supported by the observation of increased cell wall glycogen content upon brewing repitching or winemaking processes (Bastos et al., 2015; Dake et al., 2011; Reis et al., 2023). Moreover, an increase in (β1 → 4)-D-Glc linkages has been reported for several brewing yeasts upon brewing process (Bastos et al., 2015; Pinto et al., 2015; Reis et al., 2023), appearing to be an adaptation to improve yeast survival. A previous study (Bastos et al., 2015) showed that the amount of glycogen and cellulose-like polymers in the inoculum yeast was 10 %

* Corresponding authors.
E-mail addresses: ritabastos@ua.pt (R. Bastos), imarin@ua.pt (I. Marín-Montesinos), soniasferreira@ua.pt (S.S. Ferreira), fmentink@magnet.fsu.edu (F. Mentink-Vigier), msardo@ua.pt (M. Sardo), lmafra@ua.pt (L. Mafra), mac@ua.pt (M.A. Coimbra), ecoelho@ua.pt (E. Coelho).

https://doi.org/10.1016/j.carbpol.2023.121475
Received 4 August 2023; Received in revised form 16 September 2023; Accepted 8 October 2023
Available online 10 October 2023

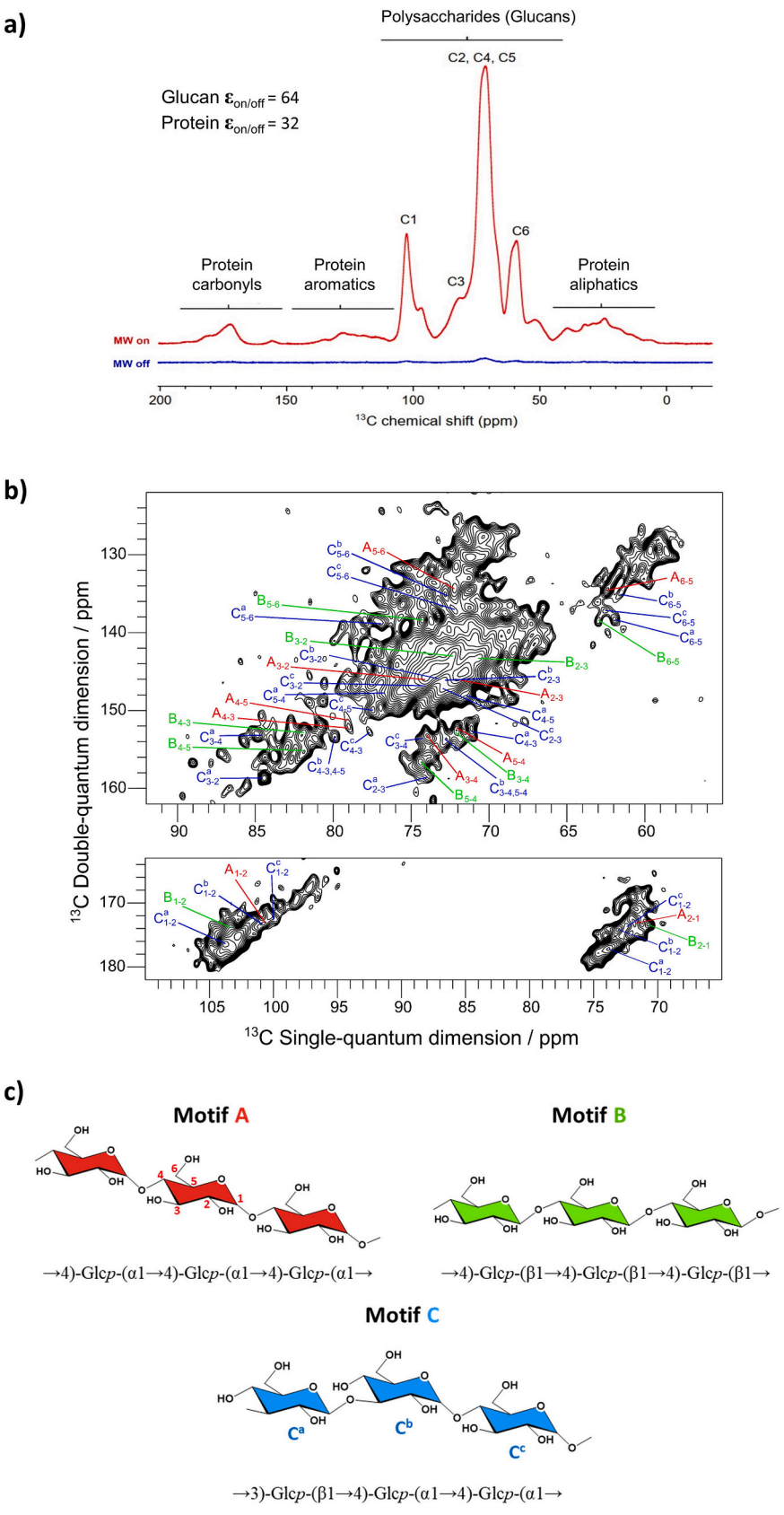

Fig. 1. ^{13}C CP MAS-DNP of AE-4M and possible structures assigned. a) Experiments performed under microwave irradiation ON (red) and OFF (blue). b) ^{13}C—^{13}C DQ/SQ CP INADEQUATE SPC-5 spectrum that provided the ^{13}C through-space connectivity for each pair of dipolar coupled carbons. c) Glucan motifs identified in AE.4M. Different motifs resonances were tagged with a colour (red, green, blue) and letter (A, B, C) code; a numbering subscript refers to the glucose unit carbons (C1, C2, C3, C4, C5, and C6) contributing to a certain correlation peak. As glucan motif C is composed of different glycosidic linkages, each residue was identified with a superscript letter. (For interpretation of the references to colour in this figure legend, the reader is referred to the web version of this article.)

Table 1
^{13}C chemical shifts (δ, ppm) of assigned glucan motifs on crude AE.4M sample. The experimental data was compared and supported with the chemical shifts available in CSDB and CCMRD databases (Supplementary Table S1). Representative chemical shifts are highlighted in bold.

Motif	Glycosyl residue	δ (ppm)					
		C1	C2	C3	C4	C5	C6
A	→4)-Glc*p*-(α1 → 4	**101.0**	72.1	73.9	**79.0**	72.0	62.3
B	→4)-Glc*p*-(β1 → 4	**103.1**	70.3	71.7	**81.5**	74.3	62.7
C[a]	→3)-Glc*p*-(β1→	**103.7**	73.5	**84.3**	71.0	76.9	61.9
C[b]	→4)-Glc*p*-(α1 → 4	**100.9**	72.9	72.5	**79.9**	72.5	61.5
C[c]	→4)-Glc*p*-(α1→	**100.0**	72.4	74.1	**77.7**	72.1	62.4

and 5 % of cell wall glucans, whereas upon repitching their amount increased to 29 % and 14 %, respectively. A thorough analysis at the atomic/molecular level of the spent yeast cell wall glucan polysaccharides is crucial for assessing yeast adaptation. This can lead to significant improvements in biotechnological processes and facilitating the establishment of structure-activity relationships towards the increase of spent yeast value.

Yeast cell wall polysaccharides are intricately intertwined within the cell wall matrix, making their extraction difficult and hindering complete structural characterization (Pinto et al., 2015). Previous works focused on characterizing chemically extracted carbohydrates, often neglecting the characterization of insoluble residues (Huang, 2008; Liu et al., 2022; Shokri et al., 2008; Varelas et al., 2016), despite their importance for yeast cell wall structure and function.

Solid-state nuclear magnetic resonance (ssNMR) is the most effective technique to obtain structural information from insoluble samples, such as cell wall polysaccharides. This frequently necessitates multidimensional correlation NMR experiments (2D/3D) requiring $^{13}C/^{15}N$ isotopic labelling strategies to overcome sensitivity issues inherent to the low natural abundance of $^{13}C/^{15}N$ isotopes (Ghassemi et al., 2022; Zhao et al., 2022). However, isotopic labelling of biological samples is challenging and costly, and often sophisticated ssNMR studies cannot be applied to unlabelled systems. Recently, Magic-Angle Spinning Dynamic Nuclear Polarization (MAS-DNP) ssNMR has emerged as a solution, enabling the ssNMR investigation of the cell wall structure in several organisms, such as plants, algae, fungi, and bacteria, while observing nuclei at their natural abundance (Chow et al., 2022; Kang et al., 2018; Kang et al., 2019; Takahashi et al., 2013; Zhao et al., 2021).

In brewer's spent yeast (BSY), it is hypothesized that the covalent linkages among cell wall polysaccharides are responsible for the insolubility of cell wall glycogen. The insoluble fraction was thus examined using various methodologies. Specific enzymatic hydrolysis procedures were performed to obtain soluble glucans or diagnostic oligosaccharides, preserving the inherent structural characteristics of the polysaccharides. A comprehensive structural analysis was accomplished by combining High-Performance Anion Exchange Chromatography (HPAEC) oligosaccharide analysis with conventional NMR in tandem with DNP-ssNMR techniques to elucidate the structural features of *S. pastorianus* BSY's alkali-insoluble glucans. For the first time, this approach unveiled a detailed profile of glycosidic linkages and branching points within these complex carbohydrate structures of BSY cell walls submitted to serial repitching.

2. Material and methods

2.1. Samples

BSY *Saccharomyces pastorianus* were provided by the Portuguese brewing company SuperBock Group. The BSY was obtained from the bottom of the fermentation reactor after six fermentation cycles. To eliminate the surplus wort, the industrial BSY sample was washed three times with water at room temperature and the BSY pellet was then collected through centrifugation at 15,000 rpm (24,652 × *g*) for 10 min at 4 °C. Subsequently, the pellet was frozen and stored at −20 °C for further use.

2.2. Isolation of BSY cell wall alkali-insoluble glucans

BSY cell wall alkali-insoluble glucans were isolated according to the sequential procedure described by Bastos et al. (2015). BSY cells were sonicated during 15 min to promote the disruption of cellular membranes. The suspension was then boiled with 80 % (*v*/v) ethanol during 10 min to remove the cellular content and other low molecular weight (MW) material thereby leading to the isolation of the BSY cell walls as an Alcohol Insoluble Residue (AIR). BSY AIR was further subjected to sequential extraction using hot water (100 °C, 15 min) followed by alkali extractions with 0.1 M, 1 M and 4 M KOH solutions at room temperature for 2 h. To prevent peeling reactions, the alkali extractions were performed with oxygen-free solutions in the presence of 20 mM of $NaBH_4$. The extraction residues were separated from the solubilized material by centrifugation, acidified to pH 5 and dialyzed with 12 kDa cut-off membranes, concentrated, frozen, and freeze-dried. The crude fraction that remained insoluble after the sequential extraction until 4 M KOH represented the BSY cell wall alkali-insoluble glucans, herein identified as AE-4M (**A**lkali **E**xtraction – **4 M** KOH).

2.3. Enzymatic hydrolysis of alkali-insoluble glucans (AE-4M)

The crude AE-4M residue was the subject of several enzymatic treatments with α-amylase (1,4-α-D-glucan glucanohydrolase, EC 3.2.1.1) from *Bacillus subtilis* 62 U/mg (Sigma-Aldrich), cellulase (1,4-β-D-glucan glucanohydrolase, EC 3.2.1.4) from *Aspergillus niger* 1.5 U/mg (Sigma-Aldrich), lichenase (endo-1,3:1,4-β-D-glucan glucanohydrolase, EC 3.2.1.73) from *Bacillus subtilis* with 250 U/mg (Megazyme), and Zymolyase® 20T (main activity of endo-1,3-β-D-glucan glucanohydrolase, EC 3.2.1.39) from *Arthrobacter luteus* with 20,000 U/g (AMS-BIO). All enzymatic hydrolyses were performed following the manufacturer recommendations of temperature and enzyme units. Enzymes were added to a well-dispersed mixture of 100 mg AE-4M in 150 mL of MilliQ water, and the hydrolyses were performed in parallel during 24 h with continuous stirring. The reactions were stopped by immersion in a boiling water bath for 10 min. The supernatants were separated from the residues by centrifugation at 24,652 ×*g*, 4 °C during 20 min, and then sequentially fractionated using centrifugal filter units with 10 kDa cut-off (Amicon® Ultra-15, Merck Milipore) and 1 kDa cut-off (Macrosep®, Pall) at 2516 × *g*, 20 °C during 20 min. The retentate was washed three times using MilliQ-water, and all obtained fractions were frozen and freeze-dried for further analyses.

2.4. Sugar and protein analyses

The monosaccharides composition of oligo- and polysaccharide samples were determined by gas chromatography flame ionization detection (GC-FID) upon 2.5 h hydrolysis in 1 M H_2SO_4 at 100 °C and derivatization to alditol acetates derivates as previously described (Bastos et al., 2015). Alditol acetates were dissolved in anhydrous acetone and analysed using a GC-FID Perkin Elmer-Clarus 400 with a capillary column DB-225 (30 m length, 0.25 mm inner diameter and 0.15 μm film thickness). The oven temperature was programmed as follows: 200 °C to 220 °C at a rate of 40 °C/min (7 min), increasing to 230 °C at a rate of 20 °C/min (1 min). The temperature of the injector was 220 °C and the detector was at 230 °C. Hydrogen was used as carrier gas at a flow rate of 1.7 mL/min. The quantification of neutral sugars was done using 2-deoxyglucose as internal standard. All analyses were performed in triplicate.

Total protein content was determined using an elemental analyser Truspec 630–200-200 with a thermal conductivity detector, and the conversion of % N to the protein content was done considering the fungi

Table 2
Enzymatic hydrolysis yield (w/w), sugar and glycosidic linkage analysis of fractions obtained after 24 h enzymatic hydrolysis of AE.4M with an α-amylase, cellulase, lichenase and zymolyase. Values between brackets correspond to data from sugar analysis determined as alditol acetates. Glycosidic linkages are expressed as mol% of partially methylated alditol acetates. CH = neutral carbohydrates; t = trace.

Glycosidic Linkage	AE.4M	α-amylase				Cellulase				Lichenase				Zymolyase			
		res	>10 kDa	1–10 kDa	<1 kDa	res	>10 kDa	1–10 kDa	<1 kDa	res	>10 kDa	1–10 kDa	<1 kDa	res	>10 kDa	1–10 kDa	<1 kDa
T-Man*p*	1.3	3.4	41.7	0.7	1.2	1.3	3.2	3.2	1.9	1.0	4.6	1.3		2.9	2.3	0.5	
2-Man*p*	1.3	2.2	15.9	0.6	0.3	0.8	1.7	1.7	0.5	0.5	3.0	0.7		0.5	1.3	0.2	
3-Man*p*	t	1.0	14.3			0.4	0.9	0.9	0.1	0.2	2.0	0.3		0.2	0.5		
6-Man*p*	0.1	0.4	1.5			0.2	0.2	0.3	0.1	0.1	0.3	0.1		0.1	0.3	0.2	
2,3-Man*p*	1.4	6.8			0.6	1.8	0.3	1.2	0.4	1.5	0.3	0.4		0.1		0.1	
2,6-Man*p*	1.0	1.7	11.6	0.4		0.6	1.7	0.9	0.2	0.4	4.6	0.2		0.3	1.5		
3,6-Man*p*	0.1	0.1						0.5		t	0.1						
2,3,4,6-Man*p*	0.1	0.4				0.3				0.3				0.4			
Total	5.3	15.9	85.0	1.8	2.1	5.5	8.1	8.8	3.2	4.2	14.9	2.9	t	4.6	6	1.0	
	(4)	(5)	(87)	(3)	(–)	(3)	(9)	(8)	(–)	(2)	(12)	(6)	(5)	(7)	(5)	(1)	
T-Glc*p*	9.5	9.3	7.7	35.3	76.3	10.3	13.9	23.1	73.2	9.8	10.4	15.1	14.6	10.5	11.7	58.9	64.9
3-Glc*p*	16.3	54.8	1.3	0.4	1.2	21.0	0.6	1.9	1.6	15.8	0.6	1.2	0.7	0.8	0.3	24.3	26.3
4-Glc*p*	57.8	1.1	1.8	31.8	11.9	50.3	62.2	40.7	12.0	56.3	62.6	77.5	82.5	73.8	69.7	5.1	3.8
6-Glc*p*	2.0	11.9	3.3	15.7	6.5	3.3	3.1	12.9	5.4	2.8	1.4	1.1	0.5	0.5	3.4	6.9	3.3
2,4-Glc*p*									0.3	1.5	0.4	0.2		0.2			
3,4-Glc*p*	0.4	0.3			0.3	0.3	0.3	0.9	0.4	0.3	0.1						
3,6-Glc*p*	3.0	4.2	1.1		0.4	3.1	2.9	4.6	1.4	2.9	2.1	0.5	0.2	1.0	0.5	3.4	1.4
4,6-Glc*p*	4.9	0.2		15.0	1.2	4.3	8.8	7.3	2.2	4.1	7.5	0.8	0.3	4.3	8.3	0.1	0.1
3,4,6-Glc*p*						0.1	0.1		0.1	0.2	0.1			0.1			
2,3,4,6-Glc*p*	0.5	1.2			0.1	1.6	0.1		0.1	1.6	t	0.2	1.1	4.1	0.1	0.2	0.1
Total	94.4	83.1	15.0	98.2	97.9	94.2	91.8	91.2	96.8	95.4	85.1	96.6	100	95.3	94.0	98.9	99.9
	(96)	(95)	(13)	(97)	(100)	(97)	(91)	(92)	(100)	(98)	(88)	(94)	(95)	(93)	(95)	(99)	(100)
4-GlcNAc*p*	0.3	1.0				0.4	0.1			0.4	0.1	0.5		0.2		0.1	0.1
Total	0.3	1.0				0.4	0.1			0.4	0.1	0.5		0.2		0.1	0.1
Total CH (mg/g)	629.0 ± 6.3	466.4 ± 2.8	189 ± 7.9	346 ± 35.6	599.0 ± 8.0	550.5 ± 25.0	599.7 ± 5.5	110 ± 7.0	619 ± 19.7	630.2 ± 5.0	641.6 ± 44.8	187.3 ± 8.6	718.6 ± 1.8	379.6 ± 0.9	943.0 ± 28.7	423.7 ± 2.7	666.6 ± 5.6
Yield % (w/w)	–	53	3	2	40	74	3	1	15	83	7	2	8	42	29	6	19
Protein (mg/g)	343.3 ± 2.1	523.7 ± 0.4	–	–	–	397.0 ± 1.5	–	–	–	408.1 ± 8.0	–	–	–	596.5 ± 5.0	–	–	–

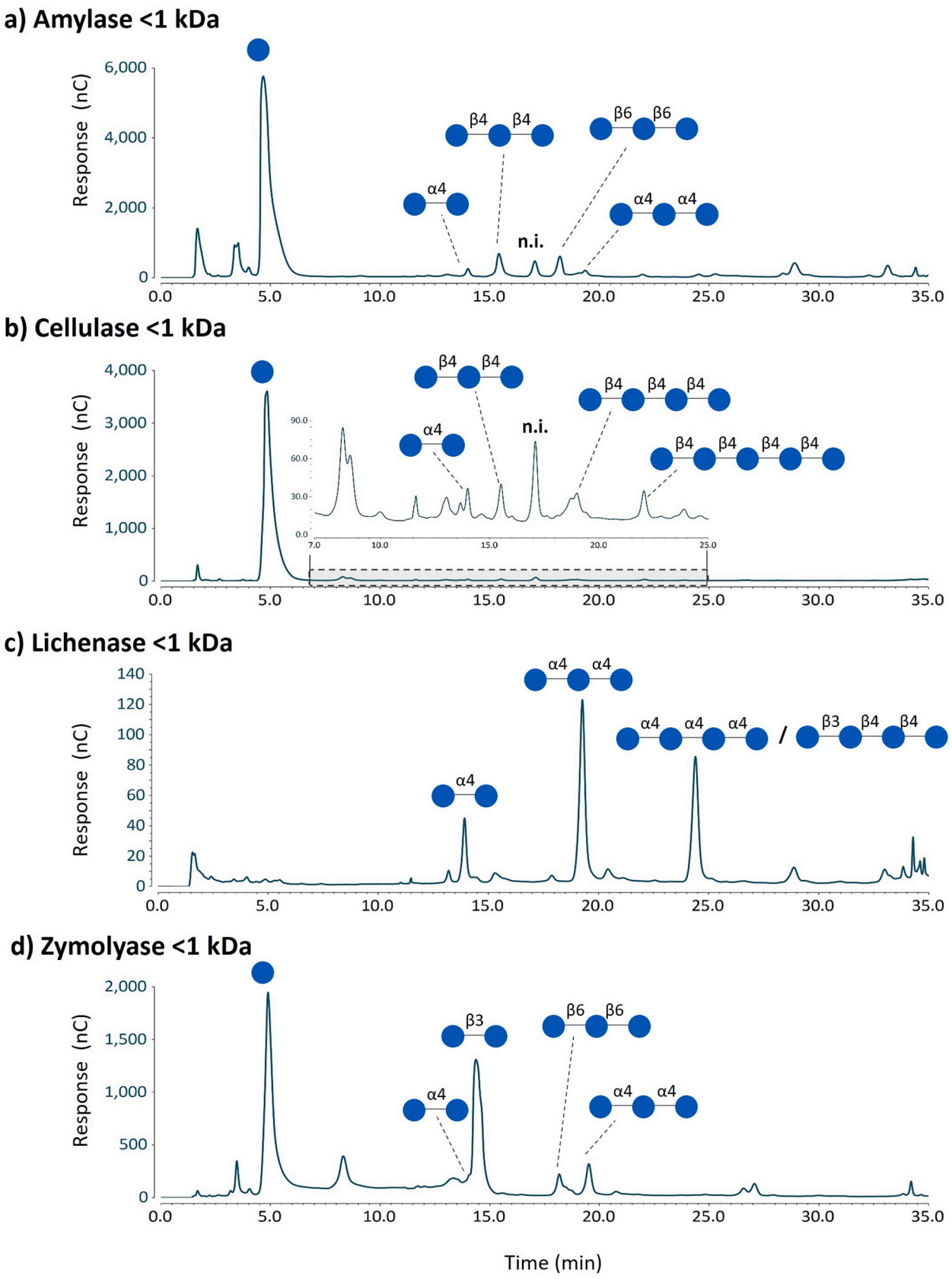

Fig. 2. HPAEC-PAD chromatograms of oligosaccharides fractions with MW lower than 1 kDa, released after a) α-amylase, b) cellulase, c) lichenase and d) zymolyase hydrolysis. Peak heights are expressed in nanocoulomb (nC); n.i. = not identified.

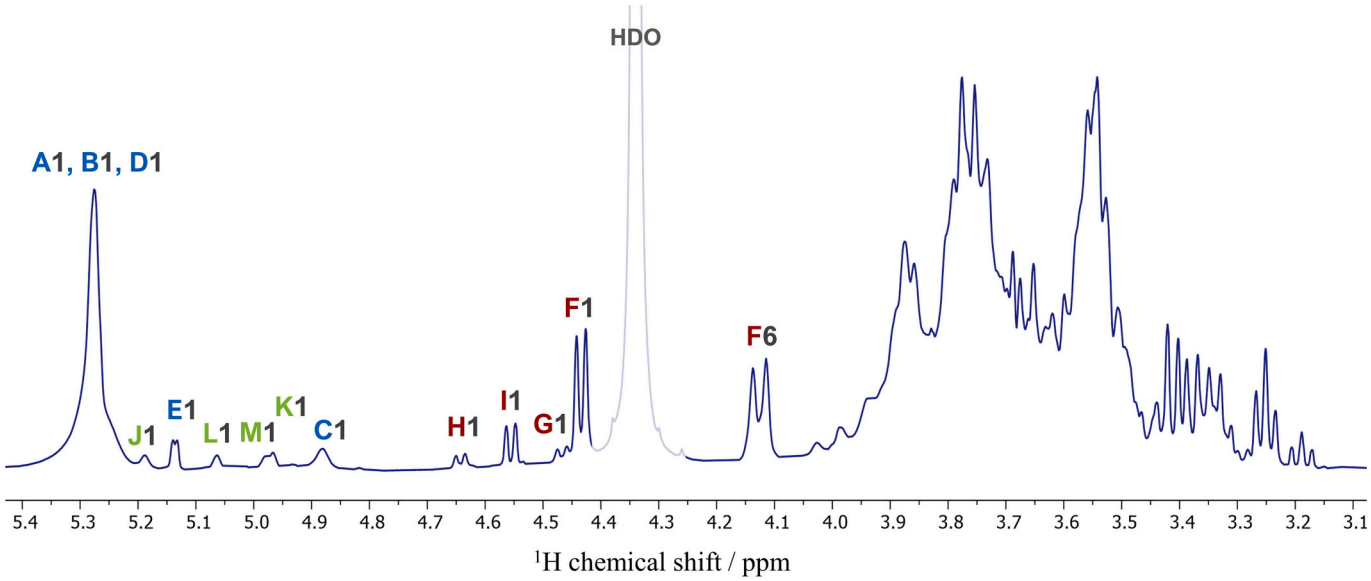

Fig. 3. ^{1}H NMR spectrum of sn.Zym > 10 kDa polysaccharide with glycosidic linkage identification using capital letters according to Table 3 followed by the carbon number. The spectrum was recorded in D_2O at 333 K at a ^{1}H Larmor frequency of 500 MHz. HDO signal was fixed at δ_H of 4.35 ppm.

Kjeldahl factor of 5.99 (Fujihara et al., 1995).

2.5. Glycosidic-linkages determined by methylation analysis

The glycosidic linkages of oligo- and polysaccharides were determined by gas chromatography-quadrupole mass spectrometry (GC-qMS) of partially methylated alditol acetate derivates (PMAA), using methyl iodide in the presence of saturated sodium hydroxide in anhydrous DMSO, as reported by Bastos et al. (2015). For polysaccharides, the methylated samples were dissolved in a chloroform methanol solution (1:1, *v*/v, 3 mL), dialysed (12 kDa cut-off membrane) against 50 % (*v*/v) of ethanol, evaporated to dryness and remethylated (to ensure the methylation of all available -OH) with the same procedure. For oligosaccharides, the samples were subjected to liquid-liquid extraction using water and dichloromethane instead of the dialysis step. All methylated samples were hydrolysed with 2 M trifluoracetic acid (TFA, 120 °C, 1 h), evaporated to dryness and reduced with sodium borodeuteride ($NaBD_4$) in 2 M NH_3. PMAA were separated and analysed by GC-qMS in a Shimadzu GCMS-QP2010 Ultra, equipped with a HT-5 capillary column (J&W Scientific, Folsom, CA, USA) capillary polyimide clad column (30 m length, 0.25 mm of internal diameter, and 0.15 μm of film thickness). The samples were injected in "split" mode using an injector temperature of 250 °C. The column oven temperature was as follows: initial temperature was 80 °C, with a linear increase of 8 °C/min until 140 °C (5 min), followed by a linear increase of 0.2 °C/min until 143.2 °C followed by a linear increase of 12 °C/min until 250 °C (1 min). The helium carrier gas had a flow rate of 1.85 mL/min and a column head pressure of 124.1 kPa. The MS analysis was performed with an ion source temperature of 250 °C, an electron impact mode at 70 eV and a scanning range of 50–600 *m/z*, 1 s cycle, in a full scan mode acquisition. PMAA were identified according to their retention times, fragmentation patterns, laboratory PMAA mass spectrum database and CCRC online database (https://www.ccrc.uga.edu/specdb/ms/pmaa/pframe.html).

2.6. High-performance anion exchange chromatography with pulsed amperometric detection (HPAEC-PAD)

Oligosaccharides recovered from Amicon® ultrafiltration separation (cut-off 1 kDa) were analysed by High-Performance Anion-Exchange Chromatography with Pulsed Amperometric Detection (HPAEC-PAD). HPAEC-PAD experiments were performed in a Dionex™ ICS-6000 system (Thermo Scientific™) equipped with a Dionex CarboPac PA100 guard column (4 mm ID × 50 mm) and a Dionex CarboPac PA100 analytical column (4 mm ID × 250 mm). Detection of carbohydrates was performed by an electrochemical detector (Dionex) with integrated amperometry mode, using AgCl reference electrode and conventional permanent gold electrode. Chromeleon 7.3 software (Thermo Scientific™ Dionex) and the standard carbohydrate quadruple waveform recommended for CarboPac columns were used. The eluents, prepared using degassed MiliQ-water, were the following: eluent A – MilliQ water (18 MΩ.cm); eluent B – 0.5 M NaOH; eluent C – 1.0 M sodium acetate (NaOAc) in 0.1 M NaOH. Commercial 50 % (*w*/w) sodium hydroxide solution (MERK) was used in eluents B and C to minimize contamination with carbonates. Eluent C was prepared by dissolution of high-grade contaminant-free sodium acetate (Thermo Scientific™ Dionex™ AAA-Direct Reagents), followed by vacuum filtration through a 0.2 μm nylon filter. All eluents were degassed by 30 min sonication and kept under nitrogen flushing in appropriate plastic Thermo Fisher Dionex eluent bottles. The eluents were kept until a maximum of one week at use. The working column and detector temperature was 30 °C. A flow rate of 1 mL/min was used with the following eluents: A:B:C (*v*/v/v) of 80:20:0, isocratically maintained for 2 min, followed by a gradient to 72:18:10 until 30.0 min, then a 25 min gradient until 0:0:100. The 100 % eluent C was maintained during 5 min. For equilibration to the next run, the eluents returned to initial ratio of 80:20:0 for 5 min and the 80 % eluent A and 20 % eluent B was maintained during 15 min.

The peak identification was done by comparing the retention time of commercial glucooligosaccharide standards (α-D-maltose, α-D-maltotriose, α-D-maltotetraose, β-D-cellobiose, β-D-cellotriose, β-D-cellotetraose, β-D-laminaribiose, β-D-laminaritriose, 6^3-α-D-Glucosyl-maltotriose, 3^2-β-D-Glucosyl-cellobiose, 3^1-β-D-Cellotriosyl-glucose, 3^3-β-D-Glucosyl-cellotriose, and 3^2-β-D-Cellobiosyl-cellobiose, all from Megazyme with >95 % purity) and oligosaccharides prepared by partial acid hydrolysis (TFA 1 M, 100 °C, 1 h) of commercial standards of amylose (Sigma-Aldrich, Quality Level 300), cellulose (Sigma-Aldrich, Quality Level 100), curdlan (Sigma-Aldrich, Quality Level 200), and pustulan (Invivogen) samples (Supplementary Figure, S1).

2.7. Liquid-state nuclear magnetic resonance (NMR)

NMR spectra of high molecular weight (HMW) material (>10 kDa) obtained upon zymolyase hydrolysis (sn.Zym > 10) were recorded at

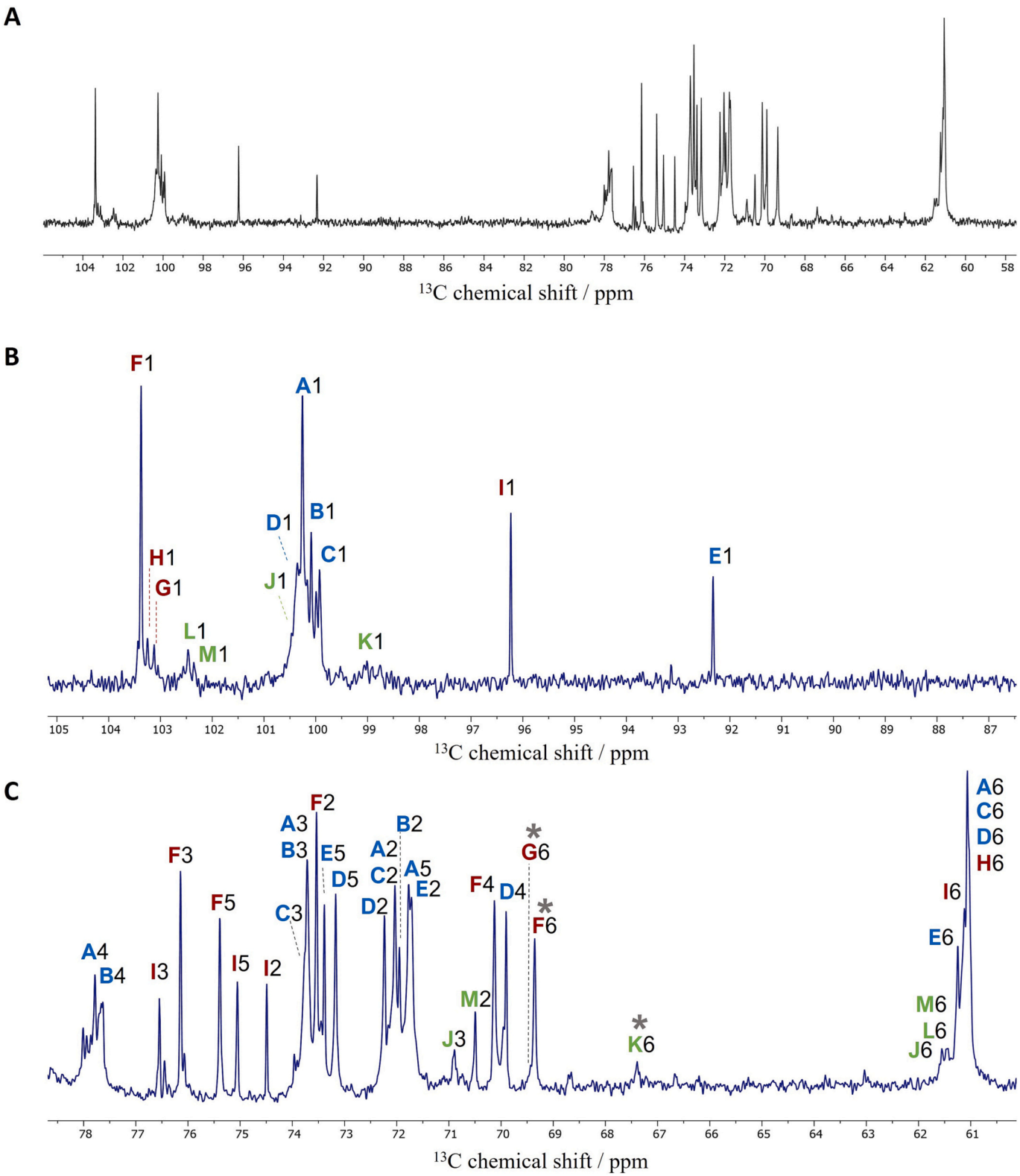

Fig. 4. (A) ^{13}C NMR spectrum of snZym>10 kDa recorded at 333 K in D_2O at a ^{1}H Larmor frequency of 125.77 MHz. (B) expansion of the anomeric region. (C) Expansion of carbinolic region. Capitals represent carbons of glycosyl residues reported in Table 3. Asterisks (*) identify the negative signals in the DEPT-135 NMR spectrum.

333 K on a Bruker DRX 500 spectrometer operating at 500.13 (^{1}H) and 125.77 (^{13}C) MHz, using D_2O as solvent. All ^{1}H and ^{13}C NMR chemical shifts are expressed in ppm (δ) and reported relative to TMS (δ 0.0 ppm). Identification was performed using the characteristic NMR chemical shifts as well as with the use of a set of 2D experiments as follows: 2D (^{1}H—^{1}H) homonuclear correlation spectroscopy (COSY), total correlation spectroscopy (TOCSY) and rotating-frame Nuclear Overhauser Effect Spectroscopy (ROESY) as well as 2D (^{1}H—^{13}C) heteronuclear single-

Table 3
^{1}H and ^{13}C chemical shifts (δ) of snZ > 10 kDa recorded at 333 K in D_2O at ^{1}H and ^{13}C Larmor frequency of 500.13 MHz and 125.77 MHz, respectively.

Glycosyl residue		δ (ppm)					
		H1 C1	H2 C2	H3 C3	H4 C4	H5 C5	H6 a/b C6
A	→4)-Glc*p*-(*α*1→	5.28	3.53	3.87	3.54	3.75	3.69/ 3.77
		100.26	72.04	73.72	**77.78**	71.71	61.07
B	→4)-Glc*p*-(*α*1 → 6	4.88	3.50	3.92	3.53	–	3.69/ 3.77
		99.07	72.04	73.72	**77.66**	–	61.07
C	→4,6)-Glc*p*-(*α*1→	5.27	3.53	3.87	3.55	–	–
		100.09	71.95	73.72	**78.01**	–	–
D	Glc*p*-(*α*1→	5.26	3.49	3.65	3.34	3.63	3.67/ 3.71
		100.35	72.23	73.76	69.91	73.21	61.03
E	→4)-*α*-Glc*p*	5.12	3.48	3.86	3.54	3.84	3.71
		92.33	71.70	73.45	77.94	69.96	61.25
F	→6)-Glc*p*-(*β*1→	4.43	3.25	3.41	3.36	3.54	3.77/ 4.14
		103.37	73.54	76.14	70.13	75.39	**69.36**
G	→3,6)-Glc*p*-(*β*1→	4.46	3.44	3.66	3.46	3.55	3.76/ 3.92
		103.25	73.96	**85.11**	68.65	76.07	**69.42**
H	Glc*p*-(*β*1→	4.64	3.28	3.44	–	–	3.67/ 3.71
		103.13	73.45	–	–	–	61.00
I	→4)-*β*-Glc*p*	4.55	3.19	3.67	3.53	3.50	3.67/ 3.77
		96.24	74.48	76.58	77.66	75.05	61.14
J	→2)-Man*p*-(*α*1→	5.20	4.01	3.85	3.60	–	–
		100.36	**78.85**	70.90	67.39	–	61.44
K	→2,6)-Man*p*-(*α*1→	5.00	3.93	–	3.71	–	3.93/–
		98.49	79.00	–	66.63	–	**66.12**
L	Man*p*-(*α*1 → 2	4.97	–	–	–	–	–
		102.46	–	–	–	–	61.55
M	Man*p*-(*α*1 → 3	5.07	3.99	–	–	–	–
		102.46	70.51	–	–	–	61.55

quantum correlation spectrum (HSQC) and heteronuclear multiple quantum coherence spectrum (HMBC). COSY was recorded with 166 transients over 256 increments (zero-filled to 1 K) and 1 K data points with spectral widths of 5000 Hz and relaxation delay of 1.0 s. HSQC with gradient pulses for selection was recorded with 144 scans, zero-filled to 1 K, a spectral width of 5000 Hz in F2 and 21,739 Hz in F1 and recycle delay of 1.5 s. A cosine multiplication was applied in both dimensions. The delays were adjusted according to the coupling constant ^{1}J(CH) of 149 Hz. HMBC with gradient pulses for selection was recorded with 198 transients over 256 increments, 1 K data points with spectral width of 5000 Hz in F2 and 27,777 Hz in F1. The relaxation delay was 1.5 s. An exponential apodization of 3 Hz was applied in both dimensions. The low-pass *J*-filter of HMBC was adjusted for an average coupling constant ^{1}J(CH) of 149 Hz. Data analysis was performed using the MestReNova-14.0.0 program (Mestrelab Research).

2.8. Magic-angle spinning dynamic nuclear polarization (MAS-DNP) ssNMR

Approximately 50 mg of samples AE.4M and zymolyase hydrolysate higher than 10 kDa (sn.Zym > 10 kDa) were impregnated with 100 μL of a 10 mM solution of Asympol-POK (Mentink-Vigier et al., 2018) radical in D_8-glycerol/D_2O/H_2O (60/30/10 vol%) following the procedure described by Kirui et al. (2019). Around 30 mg were packed in a 3.2 mm sapphire rotor for MAS-DNP experiments. The DNP experiments were performed on a 600 MHz (14.1 T)/395 GHz MAS-DNP instrument at National High Magnetic Field Laboratory, Tallahassee, Florida (Dubroca et al., 2018). All spectra were registered using a low-temperature MAS 3.2 mm probe in triple resonance mode (^{1}H/^{13}C/^{15}N). The MAS frequencies were 8 kHz and 10.5 kHz for the ^{13}C CPMAS and the ^{13}C—^{13}C dipolar INADEQUATE SPC-5 spectra, respectively (Hohwy et al., 1999). All ^{13}C chemical shifts were reported with respect to TMS. The DNP enhancement ($\varepsilon_{on/off}$) and polarization build-up time (T_b) in samples AE.4 M and sn.Zym > 10 kDa were measured using a CPMAS experiment. For both samples, the following parameters were used: recycle delay of 3 s, contact time of 1 ms, power of 38 kHz pulse in the carbon channel and a 28 kHz pulse in the proton channel with a RF ramped amplitude from 80 % to 100 %. SPINAL-64 was used for proton decoupling at a power of 100 kHz (Fung et al., 2000). A total number of 32 transients were acquired. To assign the resonances of the polysaccharide structures in sample AE.4 M and sn.Zym > 10 kDa, 2D ^{13}C—^{13}C double-quantum/single-quantum dipolar (DQ/SQ) INADEQUATE correlation experiments were performed using the SPC-5 symmetry-based pulse sequences to recouple the ^{13}C—^{13}C dipolar interaction (Hohwy et al., 1999; Karlsson et al., 2003). The recycle delay was 1.5 s and 1.8 s for samples AE.4 M and sn.Zym > 10 kDa, respectively. The CPMAS part of the pulse sequence was performed as described above. For each sample, two different mixing times were used for the SPC-5 block. To assess short distance correlations (1–3 Å), a mixing time of 0.4 ms was applied, while for longer distance (3–5 Å) contacts the mixing time was set to 0.6 ms. At MAS frequency of 10 kHz, the SPC-5 sequence uses a ^{13}C recoupling RF field of 50 kHz. The total acquisition time was approximately 33 h and a total of 128 increments were acquired in the indirect dimension for each experiment for sample AE.4 M. In the case of sample sn.Zym > 10 kDa, the total acquisition time was ~60 h.

3. Results and discussion

3.1. Characterization of yeast cell wall alkali insoluble glucans via DNP-NMR

S. pastorianus alkali-insoluble glucans are composed of distinct glycosidic linkages, including both (*α*1 → 4)- and (*β*1 → 4)-Glc linkages. These linkages seem to increase during the brewing process in detriment of (*β*1 → 3)-linked glucans (Bastos et al., 2015; Pinto et al., 2015).

After hot water and alkali sequential extraction procedure in the presence of sodium borohydride and molecular oxygen-free aqueous solutions, able to preserve the polysaccharide glycoside linkages, 23 % (*w*/w) of *S. pastorianus* BSY remained as insoluble material (AE.4 M) composed of 63 % of carbohydrates with 96 mol% of Glc. As BSY cell wall may represent 30 % of yeast dry weight (Kollár et al., 1997), at least 77 % of the cell wall remained insoluble after sequential extraction. Glycosidic linkages determined by methylation analysis revealed that AE-4M glucans were mainly composed of (1 → 4)- and (1 → 3)-linked Glc residues (57.8 and 16.3 mol%, respectively), with (1 → 4,6)-Glc (4.9 mol%) and (1 → 3,6)-Glc (3.0 mol%) branching points. Terminally linked Glc accounted for 9.5 mol% (Table 2).

Fig. 1a shows the MAS-DNP ^{13}C CPMAS spectra of BSY cell wall for AE-4M in the absence (blue) and presence (red) of microwave irradiation. The glucan resonances are clearly displayed in the region between 50 and 105 ppm (Fernando et al., 2007). Enhancement factors of 64 and 32 were obtained for unlabelled AE.4M sample on the carbohydrate and on the proteins, respectively. The enhancement on the carbohydrate is 2-fold higher than the values reported for natural-abundance experiments in plant (Zhao et al., 2021) and ^{13}C labelled fungi cell walls (Kang et al., 2018). This enhancement can be attributed to the higher performance of the AsymPol-POK radical used (Mentink-Vigier et al., 2018) and a higher crystallinity degree of the AE-4M sample, retrieved after physical reorganization upon alkali extraction procedure. The 2D ^{13}C—^{13}C DQ/SQ INADEQUATE SPC-5 spectrum of AE.4M (Fig. 1b) exhibits a very good resolution with resonances with a linewidth between 0.4 and 1 ppm, which is in agreement with MAS-DNP measurements on unlabelled plant cell wall samples (Zhao et al., 2021). This spectrum allows to unambiguously resolve and identify several key glycosidic linkages (Fig. 1c and Table 1). The assignment of each carbon resonance in the different

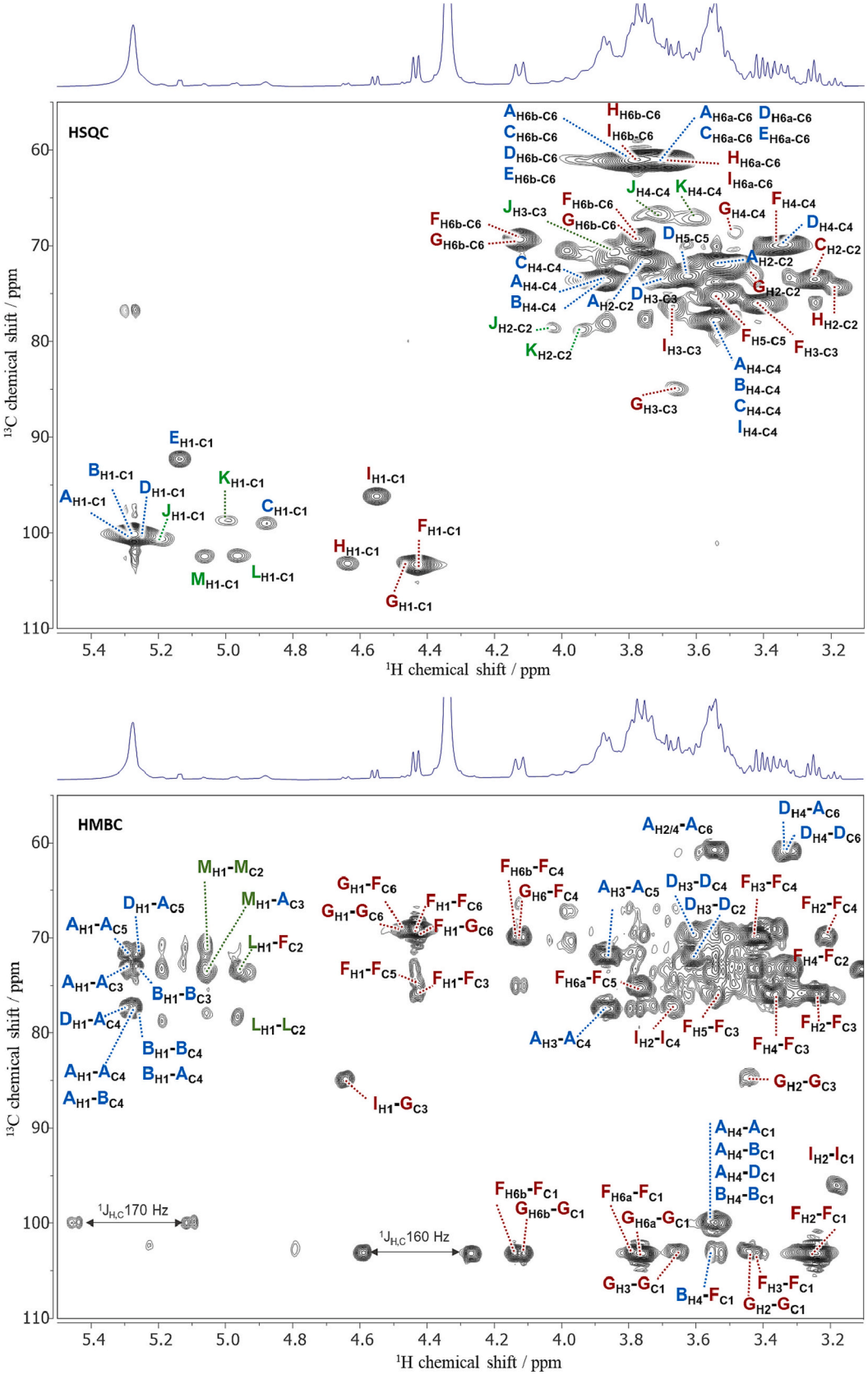

Fig. 5. HSQC and HMBC spectra of snZym>10 kDa fraction. Capitals represent the type of glycosyl residue reported in Table 3, followed by the number of carbon and proton.

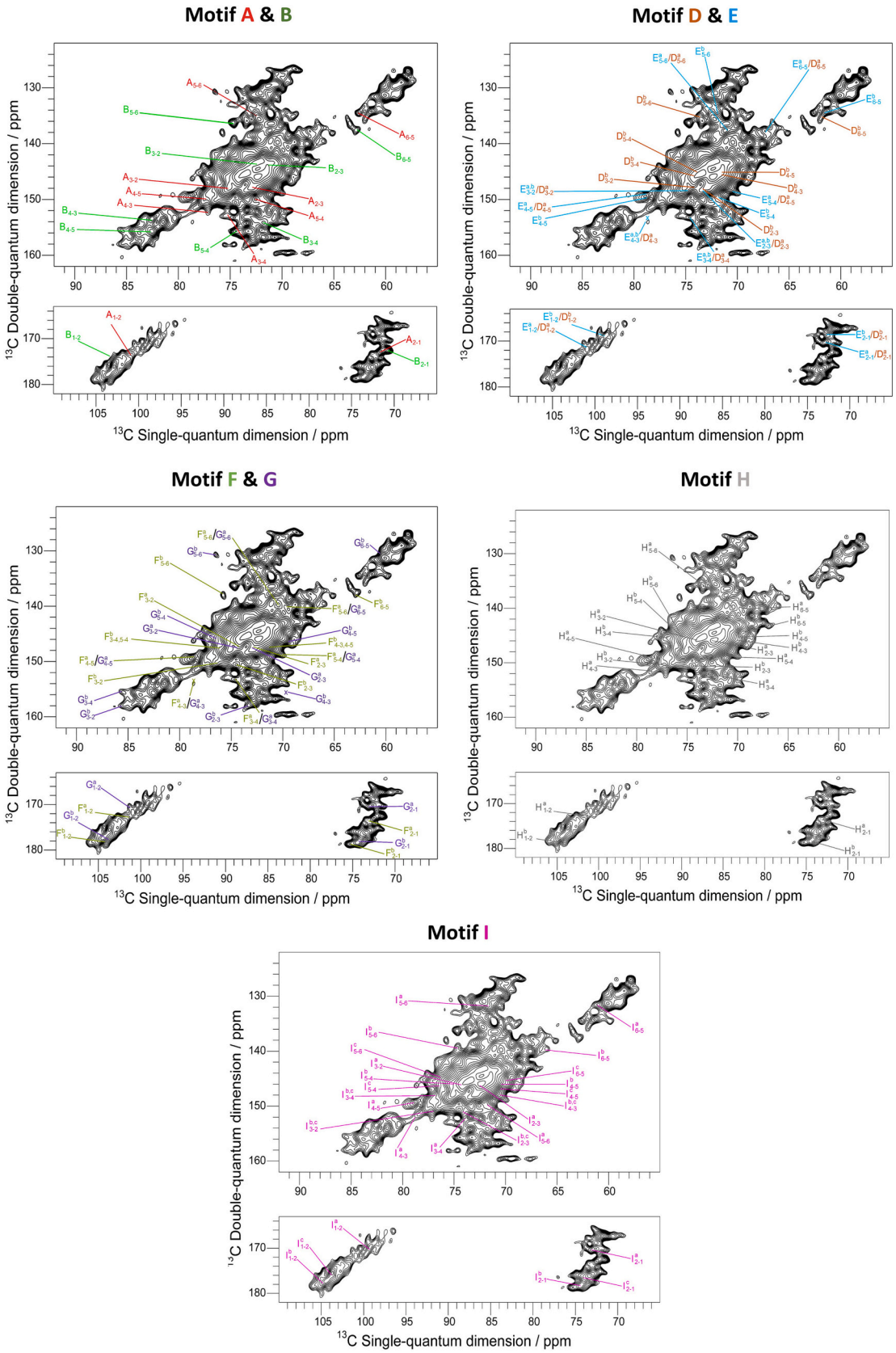

Fig. 6. 2D ^{13}C—^{13}C MAS-DNP spectrum of sn.Zym > 10 kDa with ^{13}C through-space connectivity of dipolar coupled carbons for each assigned glucan motifs (represented in Fig. 7).

Table 4
^{13}C chemical shifts (δ) of assigned glucan motifs in sample sn.Zym > 10 kDa. The experimental data was compared and supported with the chemical shifts available in CSDB and CCMRD databases (Supplementary Table S2). Representative chemical shifts are highlighted in bold.

Motif	Glycosyl residue	δ (ppm)					
		C1	C2	C3	C4	C5	C6
A	→4)-Glc*p*-(α1 → 4	**101.3**	71.7	74.9	**77.2**	72.3	62.6
B	→4)-Glc*p*-(β1 → 4	**102.9**	70.4	72.0	**82.5**	74.5	63.0
D[a]	→4,6)-Glc*p*-(α1 → 4	100.9	72.9	74.8	**78.8**	70.9	**67.3**
D[b]	Glc*p*-(α1 → 6	**99.3**	72.8	74.1	70.9	**73.6**	62.1
E[a]	→4,6)-Glc*p*-(α1 → 4	100.9	72.9	74.8	**78.8**	70.9	**67.3**
E[b]	→4)-Glc*p*-(α1 → 6	**98.6**	73.2	74.8	**78.8**	71.9	61.5
F[a]	→4,6)-Glc*p*-(α1 → 4	101.3	72.9	74.4	**78.6**	70.4	**69.6**
F[b]	Glc*p*-(β1 → 6	104.1	75.0	76.2	71.4	**76.2**	62.8
G[a]	→4,6)-Glc*p*-(α1 → 4	101.3	73.2	74.5	**78.6**	70.4	**69.6**
G[b]	→3)-Glc*p*-(β1 → 6	103.8	74.1	**85.7**	69.6	76.5	61.0
H[a]	→4,6)-Glc*p*-(α1 → 4	**101.3**	73.1	74.0	**78.5**	70.5	69.6
H[b]	→6)-Glc*p*-(β1 → 6	**103.8**	74.3	76.7	**70.2**	75.8	69.4
I[a]	→4)-Glc*p*-(α1 → 6	**99.2**	73.2	74.2	**78.7**	71.8	61.3
I[b]	→6)-Glc*p*-(β1 → 6	**104.5**	74.4	76.9	70.5	74.9	**66.2**
I[c]	→6)-Glc*p*-(β1 → 6	**103.8**	74.2	76.9	70.5	76.4	**70.1**

residues (Table 1) was assisted by the use of the Carbohydrate Structure Database (Kapaev & Toukach, 2017) and the Complex Carbohydrates Magnetic Resonance Database (Kang et al., 2020). The main signals found belong to (1 → 4)-Glc linked glucans with some contributions from (β1 → 3)-Glc, which agrees with methylation analysis of the AE.4M sample (Table 2).

A full set of ^{13}C—^{13}C correlations between all carbons (pairs C1-C2, C2-C3, C3-C4, C4-C5 and C5-C6) was found for the following glucan motifs: A) [→4)-Glc*p*-(α1→4)-Glc*p*-(α1 → 4)-Glc*p*-(α1 →], B) [→4)-Glc*p*-(β1→4)-Glc*p*-(β1 → 4)-Glc*p*-(β1 →] and C) [→3)-Glc*p*-(β1 → 4)-Glc*p*-(α1 → 4)-Glc*p*-(α1→] (Table 1 and Fig. 1c). Full correlation for motif B corroborates the occurrence of contiguous (β1 → 4)-Glc linkages, as first hypothesized by Bastos et al. (2015). In the case of motif C, a full correlation to the direct linkage of (β1 → 3)-Glc to (α1 → 4)-Glc residues through a (β1 → 4)-Glc linkage was found. This result hints towards the existence of a covalent linkage of the cell wall (β1 → 3)-glucans through a (β1 → 4)-Glc linkage as a connector to glycogen. The covalent linkage of glycogen to (β1 → 3)-glucans hypothesized to occur via (β1 → 6)-Glc linked side chain in *S. cerevisiae* cell wall (Arvindekar & Patil, 2002) was not confirmed in this yeast sample.

3.2. AE-4M enzymatic hydrolysis

To obtain a comprehensive overview of the structural features of BSY alkali insoluble glucan, AE-4M was enzymatically hydrolysed. The yields, composition, and glycosidic linkage analyses of all resulting fractions are shown in Table 2. The hydrolysis promoted by α-amylase, preferentially cleaving endo α-1,4 linkages, released 47 % of the material. Most of the solubilized material (40 %) was <1 kDa. The hydrolysis promoted by cellulase, cleaving (β1 → 4) linkages, solubilized 26 % of the material mostly with <1 kDa (15 %). After 24 h hydrolysis, AE.4M (1 → 4)-Glc decrease from 57.8 mol% to 1.1 mol% and 50.7 mol% with α-amylase and cellulase treatments, respectively. These results suggest that almost all (1 → 4)-Glc of AE.4M had α-anomeric configuration and nearly 8 % had β-configuration.

The fractions with MW higher than 10 kDa of both hydrolysates presented similar mass yield (3 %). α-Amylase hydrolysis of (α1 → 4)-Glc led to the solubilization of a fraction with low carbohydrate content (189 mg/g) and mainly composed of short chains of mannose residues (87 mol%). These results are consistent with the solubilization of cell wall type *O*-mannoproteins that have high protein moiety and short chains of (α1 → 2)- and (α1 → 3)-linked mannan (up to five units) (Bastos et al., 2022; Lesage & Bussey, 2006). Thus, a possible linkage between yeast cell wall glycogen and mannoproteins would occur directly through the mannose residues or through (β1 → 6)-Glc residues (3.3 mol%), as already described for (β1 → 3)-glucans linked to the mannoproteins moiety (Kollár et al., 1997; Stone, 2009). The treatment of AE.4M with cellulase released a fraction >10 kDa completely different from that obtained by α-amylase. This cellulase HMW hydrolysate fraction contained 60 % of carbohydrates, mainly composed of 62 mol% (1 → 4)-Glc and 8.8 mol% (1 → 4,6)-Glc. The cleavage of (β1 → 4)-Glc linkages only released part of yeast cell wall glycogen, which may be due to the presence of a direct linkage between glycogen and (β1 → 4)-Glc residues. Although in minor content, (β1 → 4)-Glc linkages may act as key connector between other major cell wall components, having a similar functionality as the reported (β1 → 6)-Glc (Nogami & Ohya, 2009). Both α-amylase and cellulase released 1–10 kDa fractions with similar composition, consistent with the release of lower MW glycogen and simultaneous (β1 → 6)-linked Glc (15.7 mol% with amylase and 12.9 % with cellulase). These results support the hypothesis that (β1 → 6)-linked glucans and glycogen can be directly linked in yeast cell wall.

As cellulase does not differentiate the contiguous glucan structures (cellulose-like structures) from those mixed-linked with (β1 → 3)-Glc residues (mixed-linkage glucans - MLG), a lichenase hydrolysis of AE.4M was used to make this distinction. Lichenase is a (1 → 3)(1 → 4)-β-D-glucan-4-glucanohydrolase (E.C. 3.2.1.73) that specifically cleaves the (β1 → 4)-Glc linkage of the 3-*O*-substituted Glc unit but does not cleave homopolymers linked through (β1 → 3)-Glc (i.e., curdlan) or (β1 → 4)-Glc (i.e., cellulose) (Dallabernardina et al., 2017; Planas, 2000). Around 17 % (*w*/w) of AE-4M was released after lichenase hydrolysis, which confirms the existence of mixed-linkage (β1 → 3)-Glc-(β1 → 4)-Glc structures. Such mixed-linkages have been reported on plant cell walls, lichens, and more recently on *Sinorhizobium meliloti*'s cell wall (Pérez-Mendoza et al., 2015). The observation of mixed-linkage (β1 → 3)-Glc-(β1 → 4)-Glc glucans is therefore the first report for the cell wall of Saccharomyces yeast.

The glycosidic linkage profile of HMW fractions obtained after hydrolysis with cellulase and lichenase were similar, mainly composed of 63 mol% (1 → 4)-Glc and 7.5 mol% (1 → 4,6)-Glc. Differences are high for the fractions with MW lower than 10 kDa, where lichenase fractions were mainly composed of (1 → 4)-Glc linkages (~ 80 mol%), lower terminally linked Glc residues (~ 15 mol%) and a ratio of total Glc to terminally linked Glc of 7.

Zymolyase (with main activity of endo-1,3-β-D-glucanohydrolase) hydrolysis led to an almost depletion of (1 → 3)-Glc linkages (Table 2). Like the hydrolysis with cellulase and lichenase, the HMW material released with zymolyase is enriched in (1 → 4)-Glc linkages (70 mol%), with (1 → 4,6)-Glc branching points (8 mol%). The hydrolysis of (β1 → 3) linkages appears to release of HMW glycogen, as observed during the hydrolysis of (β1 → 4) linkages promoted by cellulase and lichenase. These findings suggest that yeast cell wall polysaccharides were covalently linked to glycogen. The HMW fraction (>10 kDa) released with zymolyase contains the purest polysaccharide/glycogen fraction, with 94.3 % of total carbohydrates, and a release yield of 29 % (*w*/w). In addition to its role in energy storage and osmotolerance, it appears that glycogen serves as a mechanical core in BSY cell wall and is covalently linked to other components of the cell wall.

3.3. Oligosaccharides analysis by HPAEC-PAD

To address the structure of enzymatically released oligosaccharides, all samples with MW <1 kDa were analysed by HPAEC-PAD. α-Amylase hydrolysate showed the release of maltose and maltotriose (Fig. 2a). The high content of glucose confirmed the existence of exoglucanase activity of these commercial enzymes as secondary activity, which is more pronounced due to the 24 h hydrolysis period. The presence of cellotriose was also observed, which proves the direct linkage between (β1 → 4)-Glc and glycogen. Also, the identification of a (β1 → 6)-Glc trisaccharide (gentiotriose) enabled the identification of a direct linkage between (β1 → 6)-linked glucans and glycogen.

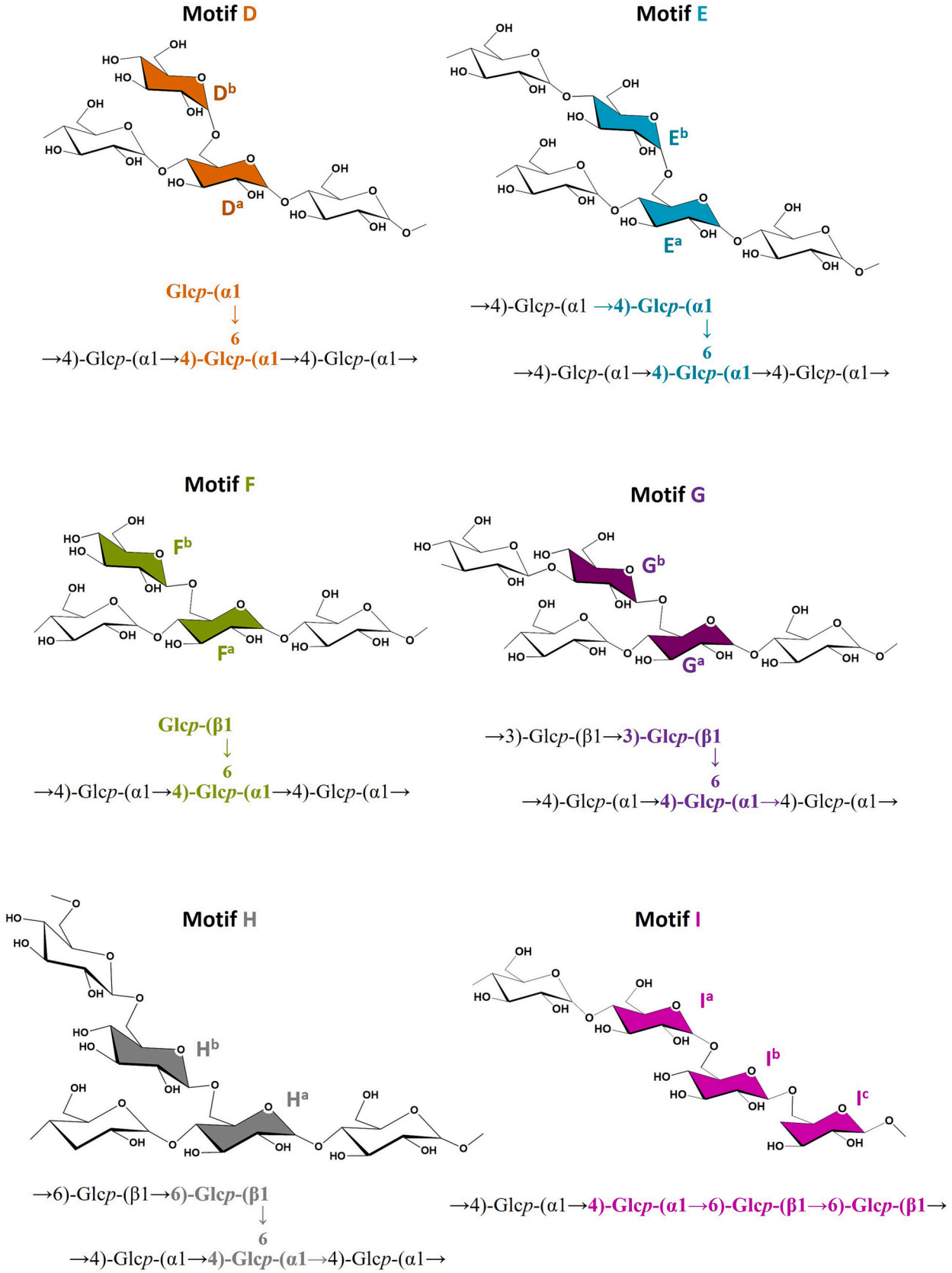

Fig. 7. Glucan motifs assigned on the 2D ^{13}C—^{13}C SQ/DQ spectrum of sn.Zym > 10 kDa obtained by MAS-DNP (Motifs A, B and C are represented in Fig. 1c). Superscript letters were used to identify motif residues that had different glycosidic linkages.

Cellulase also released a high content of glucose (Fig. 2b), as was observed for α-amylase hydrolysis. The identification of DP3-DP5 cellooligosaccharides confirmed the occurrence of contiguous (β1 → 4)-Glc linked residues in yeast cell walls, in agreement with the MAS-DNP experiments (Fig. 1). The (α1 → 4)-Glc and (β1 → 4)-Glc oligosaccharides released with both α-amylase and cellulase suggests that (α1 → 4)-Glc and (β1 → 4)-Glc can occur in the same polysaccharide structure in yeast cell wall.

Lichenase, with a specific activity of (1 → 3)(1 → 4)-β-D-glucan-4-endohydrolase, produced <1 kDa fractions with maltose (DP2) and maltotriose (DP3). Maltotetraose (DP4) and/or 3-*O*-β-glucosyl-D-cellotriose (DP4) seem to be also present. Since (1 → 3)-Glc accounted for 0.7 % whereas (1 → 4)-Glc was 82.5 %, see Table 2, one can assume that there is a much higher proportion of maltotetraose in this fraction. The absence of monomeric Glc agrees with the lower amount of terminally-linked Glc (14.6 %) than α-amylase (76.3 %) and cellulase (73.3 %) in the fractions <1 kDa (Table 2). The chromatographic profile of fraction <1 kDa obtained from lichenase (Fig. 2c) differs from the reported glucooligosaccharides released from mixed-linked glucans by lichenase. It mainly produces 3-*O*-β-cellobiosyl-D-glucose (DP3) and 3-*O*-β-cellotriosyl-D-glucose (DP4), with small amounts of DP5 to DP9 (Dallabernardina et al., 2017). These results were further corroborated using mixed-linked oligosaccharide standards, where no retention time correlation between the standards and samples was found (Supplementary Fig. S1). HPAEC-PAD results support the MAS-DNP data: (β1 → 4)-Glc acts as a key connector of (β1 → 3)-glucans and glycogen as (β1 → 3)-Glc-(β1 → 4)-Glc-(α1 → 4)-Glc motifs. The reducing end of (β1 → 3)-glucans can covalently link the C4 of glycogen through a β-linkage, which is the most stable anomeric configuration of Glc reducing end (Heyraud et al., 1979).

The extensive hydrolysis of AE.4M with zymolyase, a (β1 → 3)-endoglucanase, produced a < 1 kDa fraction mainly composed of Glc, DP2 of (β1 → 3)-Glc (laminarobiose) as well as maltose, maltotriose, and gentiotriose (Fig. 2d). These results confirmed the covalent linkage of (β1 → 3)-glucans with (β1 → 6)-glucans and glycogen.

3.4. NMR spectroscopic analysis of HMW polysaccharides released with zymolyase

The structural features of HMW (1 → 4)-Glc linked glucan fraction, released with zymolyase, sn.Zym > 10 kDa was analysed by liquid-state NMR spectroscopy and complemented with MAS-DNP solid-state NMR. Based on sn.Zym > 10 kDa methylation analysis (Table 2) and previous NMR data (Bittencourt et al., 2006; Casillo et al., 2021; Chen et al., 2014; Dinadayala et al., 2004; Han et al., 2014; Sivignon et al., 2021; Zang et al., 1990), it was possible to identify in the ^{1}H NMR spectrum (Fig. 3) the chemical shifts of α-anomeric protons from the α-glucan residues: (**A**) → 4)-Glc*p*-(α1 → at δ_H = 5.28 ppm and (**B**) → 4)-Glc*p*-(α1 → 6 at δ_H = 4.88 ppm. The branching residues (**C**) → 4,6)-Glc*p*-(α1 → (δ_H = 5.27 ppm) and terminally linked (**D**) Glc*p*-(α1 → (δ_H = 5.26 ppm) were not resolved from glycosyl residue (**A**), and only identified with 2D correlations. The well resolved doublets that appear at downfield shift between 4.4 and 4.7 ppm (Fig. 3), present a vicinal coupling constant $^{3}J_{H1,H2}$ of 7.9 Hz (large axial-axial dihedral angle) confirming the existence of β-anomeric signals (Speciale et al., 2022). The residues were identified as (**F**) → 6)-Glc*p*-(β1 → at δ_H = 4.43 ppm, (**G**) → 3,6)-Glc*p* at δ_H = 4.46 ppm, and (**H**) terminally linked Glc*p*-(β1 → residue at δ_H = 4.64 ppm. A distinct doublet was also observed at δ_H = 4.14–4.12 ppm, the most downfield shift of carbinolic region. This doublet has a large geminal constant $^{1}J_{H6,H6}$ of 11.5 Hz characteristic of deshielded H6 from a → 6)-Glc*p*-(β1 → linked residue (Benkovics et al., 2019). Minor anomeric proton signals from trace α-mannan residues were also identified between δ_H = 5.19 to 4.93 ppm, characteristic of (**J**) linear →2)-Man*p*-(α1→, (**K**) branching →2,6)-Man*p*-(α1→, and (**L, M**) terminal Man*p*-(α1 → residues.

The ^{13}C NMR spectrum (Fig. 4) main signals appear at 103.37 and 100.26 ppm. They are attributed to residues (**F**) → 6)-Glc*p*-(β1 → and (**A**) → 4)-Glc*p*-(α1→, respectively. The C6 carbons were distinguished by their negative signal in DEPT-135 NMR spectrum (Supplementary Fig. S2). The C6 carbons ($\mathbf{C}H_2$) that are not involved in glycosidic linkages appear at 61 ppm. Sugar residues that are involved in C6 glycosidic linkages appear at 69.36 ppm for C6 of residue **F** and at 69.42 ppm for C6 of residue **G**. All the assignments (Table 3) were done based on the ^{1}H—^{1}H correlations of COSY (Supplementary Fig. S3), ^{1}H—^{1}H NOESY (Supplementary Fig. S4), ^{1}H—^{1}H TOCSY spectrum (Supplementary Fig. S5), ^{13}C—^{1}H HSQC one bound correlations and ^{13}C—^{1}H HMBC intra and inter-residuals correlations (Fig. 5) experiments. With the exception of C6 of →4,6)-Glc*p*-(α1 → in the DEPT-135 spectrum, all the glycogen glycosyl residues were completely identified. The absence of C6 signal was also confirmed through the DEPT-135 spectrum of glycogen and amylopectin commercial standards, explained by the motional restriction of branching point of glycogen structures on liquid state NMR (Zang et al., 1990).

Overall, the liquid state NMR showed that zymolyase released a HMW fraction of glycogen, with minor contents of (β1 → 6)-glucans and mannans. A possible correlation between (β1 → 6)-glucans anomeric carbon and H4 from (α1 → 4,6)-Glc residues appeared in the HMBC as $\mathbf{B}_{H4}$-$\mathbf{F}_{C1}$ (Fig. 5b) and NOESY (Supplementary Fig. S4) spectra. This result may suggest a possible branching of glycogen with (β1 → 6)-glucan chains.

The MAS-DNP ssNMR 1D ^{13}C spectrum of unlabelled sn.Zym > 10 kDa (Supplementary Fig. S6) presented clear resonances of glucans between 50 and 110 ppm with negligible mannoprotein content, which agrees with the glycosidic linkage analysis (Table 2). The spectrum analysis clearly differentiated both α- and β glucosyl (1 → 4)-linked residues, which display representative resonances of anomeric carbons (δA_{C1} = 101.0 ppm and δB_{C1} = 103.1 ppm) and C4 (δA_{C4} = 77.2 ppm and δB_{C4} = 82.5 ppm) (Motif A & B Fig. 6, Table 4).

MAS-DNP was employed to investigate the occurrence of (α1 → 4,6)-Glc residues branched at C6 with a terminal α-Glc residue (Motif D, Figs. 6 and 7) or linked to other chains of (α1 → 4)-linked Glc (Motif E, Figs. 6 and 7), similar to glycogen structures. The resonances from both motifs D and E were assigned and correlated on the 2D ^{13}C—^{13}C MAS-DNP spectrum. Terminal α-Glc residue (D^b) was identified by its anomeric carbon at 99.3 ppm, showing no significant deviations related to unsubstituted glucose on other carbons, confirming the residue as a terminal α-Glc. Additionally, (α1 → 4,6)-Glc residue branched at C6 with (α1 → 4)-Glc residue were confirmed by E^b → 4)-Glc*p*-(α1 → 6 glycosyl residue C1 (98.6 ppm from (α1 → 6) linkage) and C4 to which the α-glycosidic linkage of branching chain occurs (78.8 ppm). The C4 signal of C4-C3 correlations for glycosyl residue E^a (E^a_{4-3}) and E^b (E^b_{4-3}) were barely identified. However, the signals of these two carbons were clearly observed in the C4-C5 correlations for both monomers, supporting the occurrence of branched glycogen on sn.Zym > 10 kDa. No correlation was found between the expected carbon signals of (β1 → 4,6)-Glc residues.

As branched (β1 → 4)-linked glucans were not assigned in the 2D ^{13}C—^{13}C DQ/SQ spectrum of sn.Zym > 10 kDa, it was hypothesized that (α1 → 4)-glucans might serve as branching points with terminal β-Glc residues or β-linked glucan side chains. Motif F represents the (α1 → 4)-linked glucans branched at C6 position with a terminal β-Glc residue (Fig. 7). A near complete assignment of motif F chemical shifts was achieved, missing only the C4 from C4-C3 correlation of branching residue (F^a_{4-3}), as verified for motifs D and E. As all other correlations were identified, the existence of motif F seems to be confirmed. As sn. Zym > 10 kDa was obtained through enzymatic hydrolysis of (β1 → 3)-Glc linkages, these terminal β-Glc could arise from the linkage of (β1 → 3)-glucans to glycogen via (β1 → 6)-Glc linkage, as hypothesized by Arvindekar and Patil (2002). This hypothesis was confirmed by the presence of motif G, differentiated from the branching with terminal β-Glc residue (F^b) because the C3 of residue G^b appeared at highest

chemical shift (85.7 ppm). The branching of (β1 → 6)-glucans to glycogen via (β1 → 6)-Glc linkage was also assigned as motif H, supporting the evidence found from liquid state NMR analysis. No correlation was found for the possible branching between (α1 → 4)- and (β1 → 4)-Glc linked glucans.

A full correlation for motif **I** was determined, revealing linear covalent linkage of glycogen and (β1 → 6)-glucans via a (α1 → 6) glycosidic linkage (Figs. 6 and 7). This structural motif, recently reported for *Candida albicans* cell wall, showed a covalent linkage of glycogen to (β1 → 6)-glucan side chains of (β1 → 3)-glucans (Lowman et al., 2021). The linkage of (α1 → 4)-Glc residue to (β1 → 6)-Glc through I^{a} α-C1 appeared at lower chemical shift values (99.2 ppm) when compared with α-C1 linked to other Glc secondary carbon (eg.: $A^{a}{}_{C1} = 101.0$ ppm).

4. Concluding remarks

During the brewing process, *S. pastorianus* encounters several stressful conditions due to its extended reuse (serial repitching) in successive industrial batch processes. In response, the yeasts adapt to prevent the cell rupture and death. These modifications include a reorganization of the cell wall architecture, with an increased content in glycogen. This work revealed that *S. pastorianus* brewer's spent yeast cell wall polysaccharides, namely (β1 → 3)- and (β1 → 6)-glucans, and mannoproteins are covalently linked to glycogen. The (β1 → 3)-glucans link glycogen via a (β1 → 4) glycosidic linkage, and glycogen links to (β1 → 6) linkages through a (α1 → 6) glycosidic linkage. It was also found that (β1 → 3) and (β1 → 6)-glucans can be attached to glycogen through (β1 → 6) linkages to (α1 → 4,6)-Glc residues. Glycogen exists as a constituent of the cell wall architecture, and the covalent linkages established prevent its complete extraction. Although occurring in minor content than glycogen, (β1 → 4)-Glc motifs also seem to act as key connectors within the cell wall. The cellooligosaccharides herein identified may also confer rigidity to BSY cell wall, increasing its resistance.

In conclusion, brewers spent yeast *S. pastorianus* cell wall is a complex, covalently linked structure, primarily composed of glycogen glycosidically interconnected to all other cell wall components. A comprehensive understanding of this unique BSY cell wall structure can deepen the knowledge of yeast resistance upon brewing and serial repitching. Moreover, the intricate cell wall polysaccharide framework may open up new perspectives for utilizing brewer's spent yeast in various applications, including the targeted delivery systems based on specific immune receptors and the management of fungal diseases in crops.

CRediT authorship contribution statement

Conceptualization, Elisabete Coelho (E.C.), Manuel A. Coimbra (M. A.C.); methodology, E.C., M.A.C., Ildefonso Marin-Montesinos (I.M.M.), Rita Bastos (R.B.); investigation, R.B., I.M.M., Sónia S. Ferreira (S.S.F.), Frédéric Mentink-Vigier (F.M.V.); formal analysis, R.B., I.M.M., S.S.F., F. M.V.; Validation, E.C., M.A.C., R.B., Mariana Sardo (M.S.), Luís Mafra (L. M.); Resources, E.C., M.A.C., L.M., F.M.V.; writing—original draft preparation, R.B.; writing—review and editing, E.C., M.A.C., L.M., I.M. M., F.M.V., M.S., R.B.; Visualization, R.B., I.M.M., E.C., M.A.C.; Supervision, E.C., M.A.C., I.M.M.; Project administration, E.C.; Funding acquisition, E.C., M.A.C., L.M., M.S., F.M.V.; All authors have read and agreed to the published version of the manuscript.

Declaration of competing interest

The authors declare the following financial interests/personal relationships which may be considered as potential competing interests: Professor Manuel A. Coimbra is Editor of Carbohydrate Polymers.

Data availability

Data will be made available on request.

Acknowledgments

The authors acknowledge to FCT/MEC for the financial support of the project "Yeast4FoodMed" (POCI-01-045-FEDER-030936 and PTDC/BAA-AGR/30936/2017), LAQV/REQUIMTE (UIDB/50006/2020, UIDP/50006/2020), and CICECO (UIDB/50011/2020, UIDP/50011/2020 & LA/P/0006/2020) through national funds and, where applicable, co-financed by the FEDER - Fundo Europeu de Desenvolvimento Regional, within the PT2020 Partnership Agreement. Rita Bastos was supported by an individual FCT grant (PD/BD/ 114579/2016), Elisabete Coelho thanks the research contract (CDLCTTRI-88-ARH/2018 — REF. 049-88-ARH/2018) funded by national funds (OE), through FCT, in the scope of the framework contract foreseen in the numbers 4, 5 and 6 of the article 23, of the Decree-Law 57/ 2016, of August 29, changed by Law 57/2017, of July 19. Ildefonso Marín-Montesinos is supported by the European Research Council (ERC) under the European Union's Horizon 2020 research and innovation program (Grant Agreement 865974). Mariana Sardo also acknowledges FCT for a researcher position (CEECIND/00056/2020). Thanks are also due to the Portuguese NMR Network Partnership Agreement. The authors also acknowledge Professor Artur M. S. Silva, Department of Chemistry of the University of Aveiro for helpful discussions about liquid-state NMR spectra interpretation. Thanks are also due to Super Bock Group SA (Porto, Portugal) for supplying the brewer's spent yeast samples.

The National High Magnetic Field Laboratory (NHMFL) is funded by the National Science Foundation Division of Materials Research (DMR-1644779 and DMR-2128556) and the State of Florida. A portion of this work was supported by the NIH P41 GM122698, and from the European Union's Horizon 2020 Research and Innovation Programme under grant agreement no. 101008500.

Appendix A. Supplementary data

Supplementary data to this article can be found online at https://doi.org/10.1016/j.carbpol.2023.121475.

References

Aguilar-Uscanga, B., & François, J. M. (2003). A study of the yeast cell wall composition and structure in response to growth conditions and mode of cultivation. *Letters in Applied Microbiology, 37*, 268–274.

Arvindekar, A. U., & Patil, N. B. (2002). Glycogen - a covalently linked component of the cell wall in *Saccharomyces cerevisiae*. *Yeast, 19*, 131–139.

Bastos, R., Coelho, E., & Coimbra, M. A. (2015). Modifications of *Saccharomyces pastorianus* cell wall polysaccharides with brewing process. *Carbohydrate Polymers, 124*, 322–330.

Bastos, R., Oliveira, P. G., Gaspar, V. M., Mano, J. F., Coimbra, M. A., & Coelho, E. (2022). Brewer's yeast polysaccharides — A review of their exquisite structural features and biomedical applications. *Carbohydrate Polymers, 277*, 118826.

Benkovics, G., Bálint, M., Fenyvesi, É., Varga, E., Béni, S., Yannakopoulou, K., & Malanga, M. (2019). Homo- and hetero-difunctionalized β-cyclodextrins: Short direct synthesis in gram scale and analysis of regiochemistry. *Beilstein Journal of Organic Chemistry, 15*, 710–720.

Bittencourt, V. C. B., Figueiredo, R. T., da Silva, R. B., Mourão-Sá, D. S., Fernandez, P. L., Sassaki, G. L., Mulloy, B., Bozza, M. T., & Barreto-Bergter, E. (2006). An α-glucan of *Pseudallescheria boydii* is involved in fungal phagocytosis and toll-like receptor activation. *Journal of Biological Chemistry, 281*, 22614–22623.

Casillo, A., Fabozzi, A., Russo Krauss, I., Parrilli, E., Biggs, C. I., Gibson, M. I., … Corsaro, M. M. (2021). Physicochemical approach to understanding the structure, conformation, and activity of mannan polysaccharides. *Biomacromolecules, 22*, 1445–1457.

Chen, L., Zhang, B.-B., Chen, J.-L., & Cheung, P. C. K. (2014). Cell wall structure of mushroom sclerotium (*Pleurotus tuber-regium*): Part 2. Fine structure of a novel alkali-soluble hyper-branched cell wall polysaccharide. *Food Hydrocolloids, 38*, 48–55.

Chow, W. Y., De Paëpe, G., & Hediger, S. (2022). Biomolecular and biological applications of solid-state NMR with dynamic nuclear polarization enhancement. *Chemical Reviews, 122*, 9795–9847.

Dake, M. S., Khetmalas, M. B., & Amarapurkar, S. V. (2011). Role of insoluble glycogen in ethanol adaptation mechanism of *Saccharomyces italicus*. *Indian Journal of Science and Technology, 4*, 52–55.
Dallabernardina, P., Schuhmacher, F., Seeberger, P. H., & Pfrengle, F. (2017). Mixed-linkage glucan oligosaccharides produced by automated glycan assembly serve as tools to determine the substrate specificity of Lichenase. *Chemistry – A European Journal, 23*, 3191–3196.
Dinadayala, P., Lemassu, A., Granovski, P., Cérantola, S., Winter, N., & Daffé, M. (2004). Revisiting the structure of the anti-neoplastic glucans of *Mycobacterium bovis* bacille Calmette-Guérin: Structural analysis of the extracellular and boiling water extract-derived glucans of the vaccine substrains. *Journal of Biological Chemistry, 279*, 12369–12378.
Dubroca, T., Smith, A. N., Pike, K. J., Froud, S., Wylde, R., Trociewitz, B., … Hill, S. (2018). A quasi-optical and corrugated waveguide microwave transmission system for simultaneous dynamic nuclear polarization NMR on two separate 14.1 T spectrometers. *Journal of Magnetic Resonance, 289*, 35–44.
Fernando, L. D., Zhao, W., Dickwella Widanage, M. C., Mentink-Vigier, F., & Wang, T. (2007). Solid-state NMR and DNP investigations of carbohydrates and cell-wall biomaterials. *In eMagRes*, 251–258.
Fujihara, S., Kasuga, A., Aoyagi, Y., & Sugahara, T. (1995). Nitrogen-to-protein conversion factors for some common edible mushrooms. *Journal of Food Science, 60* (5), 1045–1047.
Fung, B. M., Khitrin, A. K., & Ermolaev, K. (2000). An improved broadband decoupling sequence for liquid crystals and solids. *Journal of Magnetic Resonance, 142*, 97–101.
Ghassemi, N., Poulhazan, A., Deligey, F., Mentink-Vigier, F., Marcotte, I., & Wang, T. (2022). Solid-state NMR investigations of extracellular matrixes and cell walls of algae, bacteria, fungi, and plants. *Chemical Reviews, 122*, 10036–10086.
Gibson, B. R., Lawrence, S. J., Leclaire, J. P. R., Powell, C. D., & Smart, K. A. (2007). Yeast responses to stresses associated with industrial brewery handling. *FEMS Microbiology Reviews, 31*, 535–569.
Han, X.-Q., Yue, G.-L., Yue, R.-Q., Dong, C.-X., Chan, C.-L., Ko, C.-H., … Han, Q.-B. (2014). Structure elucidation and immunomodulatory activity of a Beta glucan from the fruiting bodies of *Ganoderma sinense*. *PLoS One, 9*, Article e100380.
Heyraud, A., Rinaudo, M., Vignon, M., & Vincendon, M. (1979). 13C-NMR spectroscopic investigation of α- and β-1,4-D-glucose homooligomers. *Biopolymers, 18*, 167–185.
Hohwy, M., Rienstra, C. M., Jaroniec, C. P., & Griffin, R. G. (1999). Fivefold symmetric homonuclear dipolar recoupling in rotating solids: Application to double quantum spectroscopy. *The Journal of Chemical Physics, 110*, 7983–7992.
Huang, G. L. (2008). Extraction of two active polysaccharides from the yeast cell wall. *Zeitschrift fur Naturforschung - Section C Journal of Biosciences, 63*, 919–921.
Kang, X., Kirui, A., Dickwella Widanage, M. C., Mentink-Vigier, F., Cosgrove, D. J., & Wang, T. (2019). Lignin-polysaccharide interactions in plant secondary cell walls revealed by solid-state NMR. *Nature Communications, 10*, 347.
Kang, X., Kirui, A., Muszyński, A., Widanage, M. C. D., Chen, A., Azadi, P., … Wang, T. (2018). Molecular architecture of fungal cell walls revealed by solid-state NMR. *Nature Communications, 9*, 2747.
Kang, X., Zhao, W., Dickwella Widanage, M. C., Kirui, A., Ozdenvar, U., & Wang, T. (2020). CCMRD: A solid-state NMR database for complex carbohydrates. *Journal of Biomolecular NMR, 74*, 239–245.
Kapaev, R. R., & Toukach, P. V. (2017). GRASS: Semi-automated NMR-based structure elucidation of saccharides. *Bioinformatics, 34*, 957–963.
Karlsson, T., Popham, J. M., Long, J. R., Oyler, N., & Drobny, G. P. (2003). A study of homonuclear dipolar recoupling pulse sequences in solid-state nuclear magnetic resonance. *Journal of the American Chemical Society, 125*, 7394–7407.
Kirui, A., Dickwella Widanage, M. C., Mentink-Vigier, F., Wang, P., Kang, X., & Wang, T. (2019). Preparation of fungal and plant materials for structural elucidation using dynamic nuclear polarization solid-state NMR. *Journal of Visualized Experiments, 2022*, Article e59152.
Klis, F. M., Boorsma, A., & De Groot, P. W. J. (2006). Cell wall construction in *Saccharomyces cerevisiae*. *Yeast, 23*, 185–202.
Kollár, R., Reinhold, B. B., Petráková, E., Yeh, H. J. C., Ashwell, G., Drgonová, J., … Cabib, E. (1997). Architecture of the yeast cell wall. *Journal of Biological Chemistry, 272*, 17762–17775.
Kwiatkowski, S., Thielen, U., Glenney, P., & Moran, C. (2009). A study of *Saccharomyces cerevisiae* cell wall glucans. *Journal of the Institute of Brewing, 115*, 151–158.
Lesage, G., & Bussey, H. (2006). Cell wall assembly in *Saccharomyces cerevisiae*. *Microbiology and Molecular Biology Reviews, 70*, 317–343.
Lillie, S. H., & Pringle, J. R. (1980). Reserve carbohydrate metabolism in *Saccharomyces cerevisiae*: Responses to nutrient limitation. *Journal of Bacteriology, 143*, 1384–1394.
Liu, J., Zhang, X., Zhang, J., Yan, M., Li, D., Zhou, S., … Liu, Y. (2022). Research on extraction, structure characterization and immunostimulatory activity of cell wall polysaccharides from *Sparassis latifolia*. *Polymers, 14*, 549.
Lowman, D. W., Sameer Al-Abdul-Wahid, M., Ma, Z., Kruppa, M. D., Rustchenko, E., & Williams, D. L. (2021). Glucan and glycogen exist as a covalently linked macromolecular complex in the cell wall of *Candida albicans* and other Candida species. *The Cell Surface, 7*, 100061.
Mentink-Vigier, F., Marin-Montesinos, I., Jagtap, A. P., Halbritter, T., van Tol, J., Hediger, S., … De Paëpe, G. (2018). Computationally assisted design of polarizing agents for dynamic nuclear polarization enhanced NMR: The AsymPol family. *Journal of the American Chemical Society, 140*, 11013–11019.
Nogami, S., & Ohya, Y. (2009). Biosynthetic enzymes for (1-3)-β-glucans, (1-3;1-6)-β-glucans from yeasts: Biochemical properties and molecular biology. In A. Bacic, G. B. Fincher, & B. A. Stone (Eds.), *Chemistry, biochemistry, and biology of 1–3 beta glucans and related polysaccharides* (pp. 259–282). San Diego: Academic Press.
Pérez-Mendoza, D., Rodríguez-Carvajal, M.Á., Romero-Jiménez, L., Farias, G.d. A., Lloret, J., Gallegos, M. T., & Sanjuán, J. (2015). Novel mixed-linkage β-glucan activated by c-di-GMP in *Sinorhizobium meliloti*. *Proceedings of the National Academy of Sciences, 112*, E757–E765.
Pinto, M., Coelho, E., Nunes, A., Brandão, T., & Coimbra, M. A. (2015). Valuation of brewers spent yeast polysaccharides: A structural characterization approach. *Carbohydrate Polymers, 116*, 215–222.
Planas, A. (2000). Bacterial 1,3-1,4-β-glucanases: Structure, function and protein engineering. *Biochimica et Biophysica Acta (BBA) - Protein Structure and Molecular Enzymology, 1543*, 361–382.
Reis, S. F., Messias, S., Bastos, R., Martins, V. J., Correia, V. G., Pinheiro, B. A., … Coelho, E. (2023). Structural differences on cell wall polysaccharides of brewer's spent Saccharomyces and microarray binding profiles with immune receptors. *Carbohydrate Polymers, 301*, 120325.
Shokri, H., Asadi, F., & Khosravi, A. R. (2008). Isolation of β-glucan from the cell wall of *Saccharomyces cerevisiae*. *Natural Product Research, 22*, 414–421.
Sivignon, A., Yu, S.-Y., Ballet, N., Vandekerckove, P., Barnich, N., & Guerardel, Y. (2021). Heteropolysaccharides from *S. cerevisiae* show anti-adhesive properties against *E. coli* associated with Crohn's disease. *Carbohydrate Polymers, 271*, 118415.
Speciale, I., Notaro, A., Garcia-Vello, P., Di Lorenzo, F., Armiento, S., Molinaro, A., … De Castro, C. (2022). Liquid-state NMR spectroscopy for complex carbohydrate structural analysis: A hitchhiker's guide. *Carbohydrate Polymers, 277*, 118885.
Stone, B. A. (2009). Chemistry of β-glucans. In A. Bacic, G. B. Fincher, & B. A. Stone (Eds.), *Chemistry, biochemistry, and biology of 1–3 beta glucans and related polysaccharides* (pp. 5–46). San Diego: Academic Press.
Takahashi, H., Ayala, I., Bardet, M., De Paëpe, G., Simorre, J.-P., & Hediger, S. (2013). Solid-state NMR on bacterial cells: Selective cell wall signal enhancement and resolution improvement using dynamic nuclear polarization. *Journal of the American Chemical Society, 135*, 5105–5110.
Varelas, V., Liouni, M., Calokerinos, A. C., & Nerantzis, E. T. (2016). An evaluation study of different methods for the production of β-D-glucan from yeast biomass. *Drug Testing and Analysis, 8*, 46–55.
Zang, L. H., Rothman, D. L., & Shulman, R. G. (1990). 1H NMR visibility of mammalian glycogen in solution. *Proceedings of the National Academy of Sciences of the United States of America, 87*, 1678–1680.
Zhao, W., Deligey, F., Chandra Shekar, S., Mentink-Vigier, F., & Wang, T. (2022). Current limitations of solid-state NMR in carbohydrate and cell wall research. *Journal of Magnetic Resonance, 341*, 107263.
Zhao, W., Kirui, A., Deligey, F., Mentink-Vigier, F., Zhou, Y., Zhang, B., & Wang, T. (2021). Solid-state NMR of unlabeled plant cell walls: High-resolution structural analysis without isotopic enrichment. *Biotechnology for Biofuels, 14*, 14.